Two-timescale magnetic attitude control of Low-Earth-Orbit spacecraft

Two-Timescale Magnetic Attitude Control of Low-Earth-Orbit Spacecraft

Giulio Avanzini[a,1], Emanuele L. de Angelis[*,b,2], Fabrizio Giulietti[b,3]

[a] *University of Salento, Lecce, Italy 73100*
[b] *University of Bologna, Forlì, Italy 47121*

Abstract

Spacecraft attitude stabilization based on active magnetic actuators represents a challenging problem, since the available control torque is constrained on a plane orthogonal to the direction of the local geomagnetic field, making the system instantaneously underactuated. A novel magnetic controller is proposed, driving a satellite flying on a Low-Earth-Orbit to three-axis stabilization on a prescribed attitude in the Nadir-pointing orbit frame. A proof of stability is provided for an idealized configuration (axisymmetric spacecraft with no disturbances). Robustness of the control technique against environmental disturbances, parameter uncertainties, corrupted measurements, and other control implementation issues is then demonstrated by numerical simulations, where the effect of magnetic residual dipoles is mitigated by online estimation.

[*]Corresponding author

[1]Professor, Department of Engineering for Innovation (DII), giulio.avanzini@unisalento.it

[2]Assistant Professor, Department of Industrial Engineering (DIN), emanuele.deangelis4@unibo.it

[3]Associate Professor, Department of Industrial Engineering (DIN), fabrizio.giulietti@unibo.it

Nomenclature

$\boldsymbol{b}$	Geomagnetic field vector expressed in $\mathbb{F}_B$, T
C_D	Spacecraft drag coefficient
$\hat{\boldsymbol{e}}_1, \hat{\boldsymbol{e}}_2, \hat{\boldsymbol{e}}_3$	Spacecraft principal axes of inertia
$\mathbb{F}_B$	Body-fixed frame
$\mathbb{F}_I$	Inertial frame
$\mathbb{F}_O$	Local-vertical/local-horizontal orbit frame
i	Orbit inclination, deg
$\boldsymbol{I}_3$	3×3 identity matrix
$\boldsymbol{J}$	Spacecraft inertia matrix, kg m^2
$k_\varepsilon, k_\zeta, \lambda$	Control gains, s^{-1}, s^{-1}, rad^{-1}
$\boldsymbol{M}$	$= (M_1, M_2, M_3)^T$ External torque acting on the spacecraft, N m
$\boldsymbol{m}$	$= (m_1, m_2, m_3)^T$ Magnetic dipole moment vector, A m^2
n	Orbit rate, rad s^{-1}
$\hat{\boldsymbol{o}}_1, \hat{\boldsymbol{o}}_2, \hat{\boldsymbol{o}}_3$	Orbital axes
r_c	Orbit radius, km
T	Orbit period, s
$\boldsymbol{T}_{BI}$	Coordinate transformation matrix between $\mathbb{F}_I$ and $\mathbb{F}_B$
$\boldsymbol{T}_{BO}$	Coordinate transformation matrix between $\mathbb{F}_O$ and $\mathbb{F}_B$
V	Velocity along the orbit, m s^{-1}
$\boldsymbol{0}_{m\times n}$	$m \times n$ zero matrix

Greek symbols

$\boldsymbol{\varepsilon}$	$= (\varepsilon_1, \varepsilon_2, \varepsilon_3)^T$ Body angular momentum error, N m s
$\boldsymbol{\omega}$	$= (\omega_1, \omega_2, \omega_3)^T$ Spacecraft angular velocity vector relative to $\mathbb{F}_I$, rad s^{-1}
$\boldsymbol{\omega}^r$	$= (\omega_1^r, \omega_2^r, \omega_3^r)^T$ Spacecraft angular velocity vector relative to $\mathbb{F}_O$, rad s^{-1}

ψ, ϕ, θ 3-1-2 Euler angle sequence, rad

ρ Air density, kg m^{-3}

$\hat{\boldsymbol{\sigma}}$ $= \boldsymbol{T}_{BO}\,(0,1,0)^T$ Unit vector along the orbit normal

$\boldsymbol{\zeta}$ $= (\zeta_1, \zeta_2, \zeta_3)^T$ Inertial angular momentum error, N m s

Subscripts

$_0$ Initial condition at time t_0

$_d$ Desired value

$_I$ Vector components in the inertial frame $\mathbb{F}_I$

$_{max}$ Maximum

$_{min}$ Minimum

$_O$ Vector components in the orbit frame $\mathbb{F}_O$

1. Introduction

Since its successful implementation in early space missions [1], magnetic actuation has turned into an attractive alternative for attitude control of spacecraft operating in Low Earth Orbit (LEO). The interest in magnetic torquers (MTs) is due to different reasons. First of all, savings in weight, cost, and complexity with respect to other systems are significant, coupled with high reliability, long operational lifetime, and use of renewable electric energy. At the same time, the possibility of a smooth modulation of control torques allows for a reduced interaction between attitude maneuvers and flexible modes [2]. The use of magnetic actuators, however, poses several problems in the selection of suitable control strategies, because the coils generate a torque that lies on a plane orthogonal to the local geomagnetic field (whose direction varies with time in the orbit frame). This makes the system

inherently underactuated, with no possibility to provide three independent control torques at each time instant [3, 4]. This causes several practical issues, ranging from the inability of tracking an arbitrary attitude to difficulties in disturbance rejection.

Full actuation can be recovered accounting for the slow variation of the local geomagnetic field along the orbit, which restores some (albeit limited) closed-loop performance on a timescale in the order of the orbital period [5]. These features make magnetic control suitable in practice for 1) small satellites with mild pointing precision requirements [6], 2) control system reconfiguration after failure (e.g., after loss of a reaction wheel in a three-axes stabilized spacecraft with no redundancy) [7], 3) spacecraft detumbling after ejection from the launch vehicle [8], and 4) momentum dumping of reaction/momentum wheels during desaturation maneuvers [9]. Conversely, when more stringent requirements on pointing accuracy are posed, mechanical devices such as reaction/momentum wheels are necessary in the presence of disturbance torques and uncertain dynamics [10].

A number of control methods have been developed for attitude acquisition, maneuver, and stabilization of magnetically actuated satellites [11, 12, 13, 14, 15]. Since the well-known B-dot control law was proposed in 1972 [16, 17], a relevant research work has focused mainly on the stability analysis of magnetic controllers. As an example, local asymptotic stability of attitude equilibrium is addressed by using either periodic optimal control in the linear case [18, 19] or time-varying controllers [20]. The problem of global asymptotic stability has also been extensively studied, but to the best of the authors' knowledge, a general solution to the problem of global magnetic at-

titude stabilization on a timescale smaller than the orbit period has not yet been derived. As a matter of fact, some papers provide encouraging results for global stabilization in the presence of sufficiently large variations of the magnetic field along one complete orbit [5, 21].

In this work, a purely-magnetic control law is presented that drives a LEO spacecraft to three-axis attitude stabilization in the orbit frame from an arbitrary initial tumbling condition. One of the most critical maneuvers for a LEO satellite platform is represented by initial attitude acquisition after release from the launch vehicle. To the best authors' knowledge, in current missions such maneuver is performed in three steps: a) a detumbling phase, which reduces the initial angular rate after deployment; b) acquisition of a pure spin condition, with spin axis along the normal to the orbit plane; c) acquisition of the desired attitude in the orbit frame. Phases a) and b) can be performed (also simultaneously) by means of a magnetic controller, whereas phase c) is usually performed by using a momentum wheel. A finite-state machine is needed for switching from one controller to the other, driving to a larger demand of computational capability.

Morevoer, a purely magnetic attitude control law for payload stabilization represents an interesting solution for low cost and/or small satellite platforms, avoiding the use of an expensive (and possibly less reliable) momentum wheel. With this objective in mind, the study investigates a control law architecture which can turn this idea into a practical solution, capable of providing full three-axis control when mechanical actuation is not available, either as a result of a design choice, aimed at minimizing complexity and cost, or in case of momentum and/or reaction wheel failure(s), thus extending the potential

operational lifetime, without the need of redundant mechanical actuation, which conversely increases weight, complexity and cost.

The proposed approach is developed within the context outlined by the same authors in [22], where a magnetically actuated spacecraft is driven to a desired pure-spin condition about a principal axis of inertia. In Ref. [23] a proof of global exponential stability was derived for a magnetic control law that simultaneously leads the satellite to 1) a spin condition around a principal axis of inertia, 2) while pointing the spin axis toward a prescribed direction in the inertial frame. In the present work, this latter approach is extended to the case of a spacecraft spinning around the pitch axis (assumed to be a principal axis of inertia), while the same is being aligned to the orbit normal. Full three-axis attitude stabilization in the orbit frame is then achieved by modulating the desired value of the pitch rate as a function of the residual pitch angle error. A two timescale behavior is forced, by means of an adequate choice of the control gains, so that the pitch angle correction task is made sufficiently slower than the spin-and-align dynamics. Three-axis stabilization is achieved and local stability for the origin of the controlled system is proven in the framework of singular perturbation analysis, which establishes robustness of stability properties for the faster dynamics [24].

The time-varying properties of the geomagnetic field in the orbit frame still play a role in the recovery of full actuation over time intervals in the order of one orbital period. In the absence of simplifying assumptions on the geomagnetic field, the proposed stability proof becomes more general with respect to studies, where a simple dipole model [18] or other particular assumptions on magnetic field play a role in the stability analysis. In such

a case, robustness against geomagnetic field model uncertainties needs to be tested, possibly leading to some performance degradation, not present in the case of the control approach developed in this paper. In spite of the local nature of the stability proof, an extensive set of Monte Carlo simulations demonstrates that convergence is achieved for any randomly generated initial attitude. Moreover, it also provides empirical evidence to the validity of a gain sizing technique proposed at the end of the stability proof.

Stability and performance of the closed-loop system are finally tested by means of numerical simulations in a realistic scenario, accounting for practical problems, which have been seldom taken care of simultaneously in previous works [25, 26]. In particular, system robustness is proven in the presence of environmental disturbances, parameter uncertainties, implementation issues [27], and actuator saturation limits [28, 29]. To this aim, the effect of large magnetic residual dipoles is mitigated by online estimation.

The main contributions of the paper and its the application scope can thus be summarized as follows: (a) a new technique for attitude stabilization by using magnetic actuators only is presented, with a potential application for any small-size satellite platform in Low-Earth Orbit; (b) a formal proof of asymptotic stability is provided, in the ideal case of axisymmetric configuration, with no environmental disturbances; (c) robustness against disturbances, model uncertainties (including three-inertial configurations with a full inertia matrix), sensors' noise and bias, actuators dynamics, and signals' quantization is demonstrated by means of an extensive set of numerical simulations; (d) the proposed control algorithm can handle all three phases of the initial satellite deployment (detumbling, spin acquisition, and attitude

acquisition), without the need for switching controllers or finite state machine; (e) a guideline for the choice of the optimal value of control gains is provided; (f) the forced first-order dynamics on the pitch angle allows for an analytical estimate of convergence time to the desired pointing attitude; (g) a more direct physical interpretation of terms is also available, if compared to averaging methods, which hinge on a considerably more complex mathematical framework.

In the next section, the mathematical model of spacecraft attitude dynamics in the presence of external disturbances is recalled. The control approach is described in the third section and closed loop performance is discussed in the next one for a realistic test case. A section of concluding remarks ends the paper.

2. System Dynamics

2.1. Angular Momentum Balance

A sketch of the spacecraft, featuring a set of mutually orthogonal MTs is represented in Fig. 1. The focus of the paper is on attitude dynamics and control, hence the orbital motion of the spacecraft center of mass is assumed to be known and only the angular momentum relative to the spacecraft center of mass is considered. All vector quantities are expressed in terms of body frame components, unless otherwise stated.

The evolution of angular velocity components is derived from the angular momentum balance equation, projected onto a frame of body axes, $\mathbb{F}_B = \{P; \hat{\boldsymbol{e}}_1, \hat{\boldsymbol{e}}_2, \hat{\boldsymbol{e}}_3\}$, fixed with respect to the spacecraft, assumed rigid, and centered in its center of mass, P:

$$\boldsymbol{J}\dot{\boldsymbol{\omega}} + \boldsymbol{\omega} \times (\boldsymbol{J}\boldsymbol{\omega}) = \boldsymbol{M} \tag{1}$$

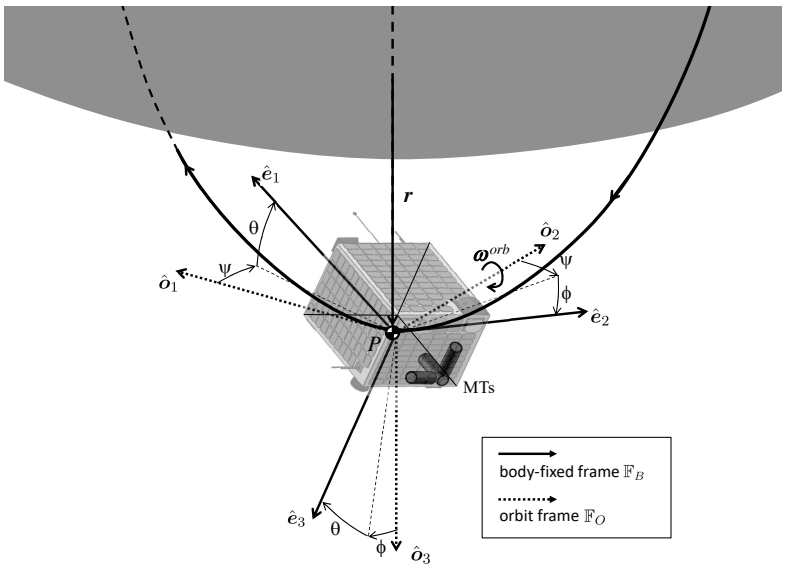

Figure 1: Sketch of spacecraft, relevant frames and 3-1-2 Euler angle sequence.

where $\boldsymbol{\omega} = (\omega_1, \omega_2, \omega_3)^T$ is the angular velocity vector of the spacecraft with respect to an inertial frame $\mathbb{F}_I = \{O; \hat{\boldsymbol{i}}_1, \hat{\boldsymbol{i}}_2, \hat{\boldsymbol{i}}_3\}$ (where O is the center of the Earth and $\hat{\boldsymbol{i}}_1$, $\hat{\boldsymbol{i}}_2$, and $\hat{\boldsymbol{i}}_3$ are three inertially–fixed unit vectors), $\boldsymbol{J} = \text{diag}(J_1, J_2, J_3)$ is the spacecraft inertia matrix (that is, $\hat{\boldsymbol{e}}_1$, $\hat{\boldsymbol{e}}_2$, and $\hat{\boldsymbol{e}}_3$ are principal axes of inertia), and $\boldsymbol{M}$ is the external torque.

The external torque, $\boldsymbol{M}$, acting on the spacecraft is the sum of magnetic and disturbance torques, $\boldsymbol{M}^{(c)}$ and $\boldsymbol{M}^{(d)}$, respectively. Magnetic control torque is $\boldsymbol{M}^{(c)} = \boldsymbol{m} \times \boldsymbol{b}$, where $\boldsymbol{m}$ is the dipole moment generated by the MTs and $\boldsymbol{b}$ is the local geomagnetic field vector, expressed in terms of body-frame components. A circular LEO of radius r_c and period T is considered, such that the orbit rate, $n = 2\pi/T$, is constant. Let $\mathbb{F}_O = \{P; \hat{\boldsymbol{o}}_1, \hat{\boldsymbol{o}}_2, \hat{\boldsymbol{o}}_3\}$ be the local-vertical/local-horizontal orbit frame, where $\hat{\boldsymbol{o}}_3$ is the vertical axis pointing towards the zenith, $\hat{\boldsymbol{o}}_2$ is normal to the orbit plane (in the direction of the orbital angular velocity), and the transverse axis $\hat{\boldsymbol{o}}_1$ completes

a right-handed triad. $\boldsymbol{b}$ is obtained from the transformation $\boldsymbol{b} = \boldsymbol{T}_{BO}\,\boldsymbol{b}_O$, where $\boldsymbol{T}_{BO}$ is the coordinate transformation matrix between $\mathbb{F}_O$ and $\mathbb{F}_B$. The components $\boldsymbol{b}_O$ of the geomagnetic field in $\mathbb{F}_O$ are derived from a suitable model, such as the tilted dipole [3, 30] or the International Geomagnetic Reference Field (IGRF) [31].

Without loss of generality, it is possible to assume $\hat{\boldsymbol{i}}_2 = \hat{\boldsymbol{o}}_2$, parallel to the normal to the orbit plane, whereas $\hat{\boldsymbol{i}}_1$ and $\hat{\boldsymbol{i}}_3$ are any pair of mutually perpendicular inertially–fixed unit vectors in the orbit plane. In this way the coordinate transformation matrix $\boldsymbol{T}_{OI}$ from $\mathbb{F}_I$ to $\mathbb{F}_O$ is equivalent to an elementary rotation matrix for a rotation around the $\hat{\boldsymbol{i}}_2 = \hat{\boldsymbol{o}}_2$ axis.

2.2. Attitude Kinematics

The attitude of the spacecraft with respect to $\mathbb{F}_O$ is described by means of an unconventional 3-1-2 Euler angle sequence, where the "yaw" angle ψ around the local vertical $\hat{\boldsymbol{o}}_3$ is given by the angular distance between $\hat{\boldsymbol{o}}_2$ and the projection of $\hat{\boldsymbol{e}}_2$ on the orbit plane. The "roll" angle ϕ is represented by the elevation of $\hat{\boldsymbol{e}}_2$ with respect to the orbit plane. The sequence of elementary rotations is completed by a "pitch" rotation θ around the unit vector $\hat{\boldsymbol{e}}_2$, as represented in Fig. 1. The transformation matrix between $\mathbb{F}_O$ and $\mathbb{F}_B$, parametrized by means of the 3-1-2 Euler angle sequence, is:

$$\boldsymbol{T}_{BO} = \begin{pmatrix} \mathrm{c}\psi\,\mathrm{c}\theta - \mathrm{s}\phi\,\mathrm{s}\psi\,\mathrm{s}\theta & \mathrm{c}\theta\,\mathrm{s}\psi + \mathrm{c}\psi\,\mathrm{s}\phi\,\mathrm{s}\theta & -\mathrm{c}\phi\,\mathrm{s}\theta \\ -\mathrm{c}\phi\,\mathrm{s}\psi & \mathrm{c}\phi\,\mathrm{c}\psi & \mathrm{s}\phi \\ \mathrm{c}\psi\,\mathrm{s}\theta + \mathrm{c}\theta\,\mathrm{s}\phi\,\mathrm{s}\psi & \mathrm{s}\psi\,\mathrm{s}\theta - \mathrm{c}\psi\,\mathrm{c}\theta\,\mathrm{s}\phi & \mathrm{c}\phi\,\mathrm{c}\theta \end{pmatrix} \tag{2}$$

provided $\mathrm{c}(\cdot) = \cos(\cdot)$ and $\mathrm{s}(\cdot) = \sin(\cdot)$. Euler angles evolve as a function of the angular speed of the spacecraft relative to $\mathbb{F}_O$, given by $\boldsymbol{\omega}^r = \boldsymbol{\omega} - \boldsymbol{T}_{BO}\,\boldsymbol{\omega}_O^{orb}$. In particular, $\boldsymbol{\omega}_O^{orb} = (0, n, 0)^T$ is the angular speed of $\mathbb{F}_O$ with

respect to the inertial frame $\mathbb{F}_I$, with components expressed in $\mathbb{F}_O$ [32]. The kinematics of yaw, roll, and pitch angles is written as a function of the angular speed of the spacecraft relative to $\mathbb{F}_O$, namely

$$\omega_1^r = \dot{\phi}\cos\theta - \dot{\psi}\cos\phi\sin\theta \tag{3}$$

$$\omega_2^r = \dot{\theta} + \dot{\psi}\sin\phi \tag{4}$$

$$\omega_3^r = \dot{\phi}\sin\theta + \dot{\psi}\cos\phi\cos\theta \tag{5}$$

or in terms of the absolute angular velocity vector of the spacecraft, $\boldsymbol{\omega} = \boldsymbol{\omega}^r + n\,\boldsymbol{T}_{BO}\hat{\boldsymbol{o}}_2$:

$$\omega_1 = \dot{\phi}\cos\theta - \dot{\psi}\cos\phi\sin\theta + n\ (\cos\theta\sin\psi + \sin\phi\sin\theta\cos\psi) \tag{6}$$

$$\omega_2 = \dot{\theta} + \dot{\psi}\sin\phi + n\ \cos\phi\cos\psi \tag{7}$$

$$\omega_3 = \dot{\phi}\sin\theta + \dot{\psi}\cos\phi\cos\theta + n\ (\sin\theta\sin\psi - \sin\phi\cos\theta\cos\psi) \tag{8}$$

In the latter case, the kinematics of Euler angles in Eqs. (6), (7), and (8) is conveniently rearranged as follows:

$$\dot{\psi} = (-\omega_1\ \sin\theta + \omega_3\ \cos\theta + n\ \sin\phi\cos\psi)\,/\,\cos\phi \tag{9}$$

$$\dot{\phi} = \omega_1\ \cos\theta + \omega_3\ \sin\theta - n\ \sin\psi \tag{10}$$

$$\dot{\theta} = \omega_2 + (\omega_1\ \sin\phi\sin\theta - \omega_3\ \sin\phi\cos\theta - n\cos\psi)\,/\,\cos\phi \tag{11}$$

The use of Euler angles deserves some attention, since any sequence of three elementary rotations is affected by singular configurations [32]. In the present case, when the second rotation ϕ is equal to ± 90 deg, the pitch axis $\hat{\boldsymbol{e}}_2$ coincides with the local vertical $\hat{\boldsymbol{o}}_3$, and the first and third rotations are performed around the same axis. This situation is unlikely to be encountered

in practice, for the rotation sequence here adopted. In fact, after a spacecraft is injected into its orbit, an initial detumbling maneuver is performed in order to dump the angular momentum accumulated during payload ejection. During this phase, when the attitude information is not yet available, because of the high rotation rates, the spacecraft is typically driven toward a pure spin condition by means of some purely magnetic control law. When a B-dot control law is adopted [16], the principal axis of maximum inertia gets sufficiently close to the normal to the orbit plane, but different control techniques are available for aligning any principal axis of inertia to the orbit normal [22]. Small values of the angles ψ and ϕ can thus be attained. This means that $\phi = \pm 90$ deg is an unlikely situation and the applicability of the control law described in this paper is not at stake.

Conversely, when a residual pitch rate is expected, both the classical yaw-pitch-roll (3-2-1) and precession-nutation-spin (3-1-3) sequences will approach singular configurations during the satellite motion, thus harming practical applicability of the control law and possibly hindering the search for closed-loop stability proofs. This motivates the choice of this unusual Euler angle sequence in the description of attitude kinematics.

2.3. Disturbance Torques

In order to assess robustness of the control laws proposed in the next section, the four most relevant sources of external disturbance torque $\boldsymbol{M}^{(d)}$ in LEO are included in the simulation model discussed in the Results section: gravity gradient, residual magnetic, aerodynamic, and solar radiation pressure torques [3]. For a circular orbit, gravity gradient torque is [32]:

$$\boldsymbol{M}^{(gg)} = 3\, n^2 \left[\hat{\boldsymbol{o}}_3 \times (\boldsymbol{J}\hat{\boldsymbol{o}}_3)\right] \tag{12}$$

The torque on the spacecraft due to the interaction of the Earth's magnetic field $\boldsymbol{b}$ with spacecraft residual magnetic dipole moment $\boldsymbol{m}_{rm}$, generated by on-board electrical systems and circuits, is given by

$$\boldsymbol{M}^{(rm)} = \boldsymbol{m}_{rm} \times \boldsymbol{b} \tag{13}$$

The interaction of the upper atmosphere molecules with the external surface of the satellite introduces an aerodynamic torque $\boldsymbol{M}^{(a)} = \boldsymbol{r}_{cp} \times \boldsymbol{F}^{(a)}$, where $\boldsymbol{r}_{cp}$ is the position of the center of pressure with respect to the center of mass of the satellite, evaluated according to the approach used in [3], and $\boldsymbol{F}^{(a)}$ is the atmospheric drag force. A simplified model is considered for $\boldsymbol{F}^{(a)} = -0,5\,\rho\,V^2\,A\,C_D\,\hat{\boldsymbol{o}}_1$, where ρ is the density of rarefied air at the considered orbit altitude, A is the spacecraft cross-sectional area, and C_D is the drag coefficient. Velocity of P with respect to the air is assumed equal to the speed along the orbit, $V = n\,r_c$.

A solar radiation pressure torque is also present, $\boldsymbol{M}^{(srp)} = \boldsymbol{r}_{srp} \times \boldsymbol{F}^{(srp)}$, where $\boldsymbol{r}_{srp}$ is the vector from spacecraft center of mass to the solar radiation center of pressure [3]. The solar radiation pressure force $\boldsymbol{F}^{(srp)}$ is written as [33] $\boldsymbol{F}^{(srp)} = -(\Phi_s/c)(1+q_s)A_s\cos(i_s)\,\hat{\boldsymbol{s}}$, where Φ_s is the solar flux density constant, adjusted for actual distance from the Sun (average value: 1367 W/m^2), $c \approx 3 \cdot 10^8$ m/s is the speed of light, and q_s is the reflectance factor (ranging from 0 for perfect absorption to 1 for perfect reflection). A worst case scenario is considered where the sunlit surface area A_s is assumed to be a constant equal to the maximum projection area of the spacecraft solid shape [34], upon which the angle of incidence of the radiation, i_s, is assumed to be zero. As a minor simplification in the simulated environment, no eclipse phase is considered. Finally, $\hat{\boldsymbol{s}}$ is the unit vector representing the direction

of the Sun, assumed to be fixed in the inertial frame and directed from the spacecraft to the Sun.

3. Attitude Stabilization

3.1. Control Law

The spacecraft attitude stabilization problem in the orbit frame $\mathbb{F}_O$ is addressed in an ideal scenario, first, with no external disturbance $\boldsymbol{M}^{(d)}$ (so that the external torque acting on the spacecraft coincides with the magnetic control torque, $\boldsymbol{M} = \boldsymbol{M}^{(c)}$), and assuming an axisymmetric inertia tensor (with the pitch axis assumed as the symmetry axis).

Letting $\hat{\boldsymbol{\sigma}} = \boldsymbol{T}_{BO}\,(0,1,0)^T$ be the unit vector parallel to $\hat{\boldsymbol{o}}_2$, fixed in both the orbit and inertial frames, two desired angular momentum vectors, $\boldsymbol{h}_d$ and $\boldsymbol{H}_d$, are introduced in the body-fixed and in the inertial frames, respectively. The first one is defined as $\boldsymbol{h}_d = (0, \eta(\theta), 0)^T$, which requires that the angular momentum vector becomes parallel to the symmetry axis, $\hat{\boldsymbol{e}}_2$. The second, $\boldsymbol{H}_d = \eta(\theta)\,\hat{\boldsymbol{\sigma}}$, requires that the angular momentum points along the (inertially–fixed) orbit normal, $\hat{\boldsymbol{o}}_2$. The linear function $\eta(\cdot) : \mathbb{R} \to \mathbb{R}$ is

$$\eta(\theta) = J_2\, n\ (1 - \lambda\, \theta) \tag{14}$$

with λ being a strictly positive parameter. Correspondingly, two different angular momentum error variables are introduced, namely

$$\boldsymbol{\zeta} = \boldsymbol{H}_d(\theta) - \boldsymbol{J}\,\boldsymbol{\omega} \tag{15}$$

and

$$\boldsymbol{\varepsilon} = \boldsymbol{h}_d(\theta) - \boldsymbol{J}\,\boldsymbol{\omega} \tag{16}$$

where all vector quantities, including $\boldsymbol{H}_d(\theta)$, are expressed in terms of body frame components [23]. The magnetic control law proposed is:

$$\boldsymbol{M}^{(c)} = \left(\boldsymbol{I}_3 - \hat{\boldsymbol{b}}\,\hat{\boldsymbol{b}}^T\right)\,(k_\zeta\,\boldsymbol{\zeta} + k_\varepsilon\,\boldsymbol{\varepsilon}) \tag{17}$$

where k_ζ and k_ε are positive gains, and $\hat{\boldsymbol{b}} = \boldsymbol{b}/||\boldsymbol{b}||$ is the unit vector parallel to the local geomagnetic field. The control torque is thus proportional to a combination of the error signals for the deviation of the current value of the angular momentum from its desired values in the inertial and in the body frame. The projection operator $\left(\boldsymbol{I}_3 - \hat{\boldsymbol{b}}\,\hat{\boldsymbol{b}}^T\right)$ accounts for the fact that no control torque is delivered around the direction of $\hat{\boldsymbol{b}}$.

From the definition of the error in Eq. (15) and taking into account the control law in Eq. (17), one has

$$\dot{\boldsymbol{\zeta}} = -\left(\boldsymbol{I}_3 - \hat{\boldsymbol{b}}\,\hat{\boldsymbol{b}}^T\right)\,(k_\zeta\,\boldsymbol{\zeta} + k_\varepsilon\,\boldsymbol{\varepsilon}) + \boldsymbol{\omega} \times (\boldsymbol{H}_d - \boldsymbol{\zeta}) + \dot{\boldsymbol{H}}_d \tag{18}$$

while the body frame angular momentum error dynamics achieves the form:

$$\dot{\boldsymbol{\varepsilon}} = -\left(\boldsymbol{I}_3 - \hat{\boldsymbol{b}}\,\hat{\boldsymbol{b}}^T\right)\,(k_\zeta\,\boldsymbol{\zeta} + k_\varepsilon\,\boldsymbol{\varepsilon}) + \boldsymbol{\omega} \times (\boldsymbol{h}_d - \boldsymbol{\varepsilon}) + \dot{\boldsymbol{h}}_d \tag{19}$$

3.2. Stability Analysis

Let the inverse of the inertia matrix, $\boldsymbol{J}^{-1}$, be the sum of two contributions. The first is related to an axisymmetric configuration, $\boldsymbol{J}_a^{-1} = \mathrm{diag}(1/J_t, 1/J_s, 1/J_t)$, where $J_s,\ J_t \in \mathbb{R}^+$ and $J_s \neq J_t$. The second is a perturbation term such that $\boldsymbol{J}^{-1} = \boldsymbol{J}_a^{-1} + \boldsymbol{\Delta}$, provided $\boldsymbol{\Delta} = \mathrm{diag}(\delta_1, \delta_2, \delta_3)$, $\delta_1\,, \delta_2\,, \delta_3 \in \mathbb{R}$. Without loss of generality, it is assigned $J_s = J_2$ and $J_t = (J_1 + J_3)/2$. In this case, one has $\delta_2 = 0$, $\delta_1 = \gamma/J_1$ and $\delta_3 = -\gamma/J_3$, where $\gamma = (J_3 - J_1)/(J_1 + J_3)$.

Spacecraft attitude dynamics is usually formulated in terms of body-frame components, that is, in the reference frame where relevant quantities are measured by on-board sensors to generate the required feedback. This motivates

the use of $\mathbb{F}_B$ for introducing all relevant vector quantities. Nonetheless, the analysis of the momentum-management problem turns out to be remarkably simpler if error dynamics in Eqs. (18) and (19) is represented in terms of components in the inertial frame $\mathbb{F}_I$. Letting $\boldsymbol{Z} = \boldsymbol{T}_{BI}^T \boldsymbol{\zeta} = \eta(\theta)\, \hat{\boldsymbol{o}}_2 - \boldsymbol{h}_I$ ($\boldsymbol{h}_I = \boldsymbol{T}_{BI}^T \boldsymbol{J}\boldsymbol{\omega}$ being the angular momentum vector expressed in $\mathbb{F}_I$) and $\boldsymbol{E} = \boldsymbol{T}_{BI}^T \boldsymbol{\varepsilon}$, provided that $\boldsymbol{T}_{BI} = \boldsymbol{T}_{BO}\, \boldsymbol{T}_{OI}$ (where $\boldsymbol{T}_{OI}$, related to orbital motion, is a function of time only), the system describing the angular momentum error dynamics becomes:

$$\dot{\boldsymbol{Z}} = -\left[\boldsymbol{T}_{BI}^T \left(\boldsymbol{I}_3 - \hat{\boldsymbol{b}}\, \hat{\boldsymbol{b}}^T\right) \boldsymbol{T}_{BI}\right] (k_\zeta\, \boldsymbol{Z} + k_\varepsilon\, \boldsymbol{E}) + \dot{\eta}\, \hat{\boldsymbol{o}}_2 \tag{20}$$

$$\begin{aligned} \dot{\boldsymbol{E}} = &-\left[\boldsymbol{T}_{BI}^T \left(\boldsymbol{I}_3 - \hat{\boldsymbol{b}}\, \hat{\boldsymbol{b}}^T\right) \boldsymbol{T}_{BI}\right] (k_\zeta\, \boldsymbol{Z} + k_\varepsilon\, \boldsymbol{E}) \\ &- \boldsymbol{T}_{BI}^T \left\{\left[\left(\boldsymbol{J}_a^{-1} + \boldsymbol{\Delta}\right) \boldsymbol{T}_{BI} \boldsymbol{E}\right] \times \boldsymbol{h}_d\right\} + \boldsymbol{T}_{BI}^T\, \dot{\boldsymbol{h}}_d \end{aligned} \tag{21}$$

Note that, in Eq. (20), the term $\dot{\boldsymbol{T}}_{OI}^T (0,1,0)^T = (0,0,0)^T$, thanks to the choice of the inertial frame described at the end of subsection 2.1. Given $\boldsymbol{Y} = \left(\boldsymbol{Z}^T, \boldsymbol{E}^T\right)^T$, $\boldsymbol{Y} \in \mathbb{R}^6$, the system in Eqs. (20) and (21) achieves the form

$$\dot{\boldsymbol{Y}} = -\boldsymbol{A}(t) \boldsymbol{K}\, \boldsymbol{Y} - \eta(\theta) \left[\boldsymbol{B}\left(t, \boldsymbol{Y}\right) + \boldsymbol{C}\left(t, \boldsymbol{Y}\right)\right] - \dot{\eta}\, \boldsymbol{D}\left(t, \boldsymbol{Y}\right) \tag{22}$$

where

$$\boldsymbol{A}(t) = \begin{pmatrix} \boldsymbol{T}_{BI}^T \left(\boldsymbol{I}_3 - \hat{\boldsymbol{b}}\, \hat{\boldsymbol{b}}^T\right) \boldsymbol{T}_{BI} & \boldsymbol{T}_{BI}^T \left(\boldsymbol{I}_3 - \hat{\boldsymbol{b}}\, \hat{\boldsymbol{b}}^T\right) \boldsymbol{T}_{BI} \\ \boldsymbol{T}_{BI}^T \left(\boldsymbol{I}_3 - \hat{\boldsymbol{b}}\, \hat{\boldsymbol{b}}^T\right) \boldsymbol{T}_{BI} & \boldsymbol{T}_{BI}^T \left(\boldsymbol{I}_3 - \hat{\boldsymbol{b}}\, \hat{\boldsymbol{b}}^T\right) \boldsymbol{T}_{BI} \end{pmatrix} \in \mathbb{R}^{6\times 6} \tag{23}$$

is a time-dependent matrix,

$$\boldsymbol{K} = \begin{pmatrix} k_\zeta\, \boldsymbol{I}_3 & \boldsymbol{0}_{3\times 3} \\ \boldsymbol{0}_{3\times 3} & k_\varepsilon\, \boldsymbol{I}_3 \end{pmatrix} \in \mathbb{R}^{6\times 6} \tag{24}$$

is a gain matrix,

$$\begin{aligned}\boldsymbol{B}\,(t,\boldsymbol{Y}) &= \begin{pmatrix} \boldsymbol{0}_{3\times 1} \\ \boldsymbol{T}_{BI}^{T}\left[\left(\boldsymbol{J}_{a}^{-1}\boldsymbol{T}_{BI}\boldsymbol{E}\right)\times\hat{\boldsymbol{e}}_{2}\right] \end{pmatrix} \\ \boldsymbol{C}\,(t,\boldsymbol{Y}) &= \begin{pmatrix} \boldsymbol{0}_{3\times 1} \\ \boldsymbol{T}_{BI}^{T}\left[\left(\boldsymbol{\Delta}\,\boldsymbol{T}_{BI}\boldsymbol{E}\right)\times\hat{\boldsymbol{e}}_{2}\right] \end{pmatrix}\end{aligned} \tag{25}$$

are gyroscopic coupling terms, and

$$\dot{\eta}\,\boldsymbol{D}\,(t,\boldsymbol{Y}) = \begin{pmatrix} \dot{\eta}\,\hat{\boldsymbol{o}}_{2} \\ \boldsymbol{T}_{BI}^{T}\,(\dot{\eta}\,\hat{\boldsymbol{e}}_{2}) \end{pmatrix} = \dot{\eta}\begin{pmatrix} \hat{\boldsymbol{o}}_{2} \\ \boldsymbol{T}_{BI}^{T}\,\hat{\boldsymbol{e}}_{2} \end{pmatrix} \tag{26}$$

is related to the time derivative of the magnitude of the desired angular momentum, with $\dot{\eta} = -\lambda\, J_2\, n\, \dot{\theta}$.

For the aim of the present analysis, the dynamics of the pitch angle is also expressed as a function of the angular momentum error variable $\boldsymbol{Y}$. Taking into account the definitions of $\boldsymbol{E}$, $\boldsymbol{Z}$, and $\boldsymbol{Y}$, it is straightforward to re-write Eq. (11) as:

$$\dot{\theta} = \boldsymbol{Q}\,\left(\boldsymbol{h}_{d}(\theta) - \boldsymbol{T}_{BI}\,\boldsymbol{S}\,\boldsymbol{Y}\right) - n\,\frac{\cos\psi}{\cos\phi} \tag{27}$$

where

$$\boldsymbol{Q} = \left(\tan\phi\,\sin\theta/J_1,\ 1/J_2,\ -\cos\theta\,\tan\phi/J_3\right) \in \mathbb{R}^{1\times 3}$$

and $\boldsymbol{S} = \left(\boldsymbol{0}_{3\times 3}\ \boldsymbol{I}_{3}\right) \in \mathbb{R}^{3\times 6}$.

In what follows, it is shown that the origin of the closed-loop system in Eqs. (22) and (27) corresponds to the condition in which spacecraft attitude is three-axis stabilized in the orbit frame. Exponential stability is addressed by the following Lemma, provided that $\gamma = 0$, namely the spacecraft has axisymmetric inertia properties about $\hat{\boldsymbol{e}}_2$.

Lemma 1 *Consider the nonlinear time-varying system in Eqs.* (22) *and* (27)*, with* $\gamma = 0$*. There exist* λ*,* k_ζ*, and* k_ε *such that the origin* $(\mathbf{Y}^T, \theta)^T = \mathbf{0}_{7\times 1}$ *is exponentially stable.*

Proof: See Appendix A.

Remark 1 According to the stability proof, the requirements on control gains and the particular choice of the control signal in Eq. (17) are selected in order to artificially provide the error dynamics in Eqs. (22) and (27) with a two-timescale behavior [35]. In the present case, the control effort related to k_ζ and k_ε makes the spacecraft acquire a pure spin condition around the pitch axis, while aiming the same axis along the orbit normal. Such a maneuver is characterized by a (relatively) fast transient, whereas the spin rate approximately tracks the desired value $n\,(1 - \lambda\,\theta)$, which depends on the residual pitch angle. If λ is designed in order to make the pitch angle correction task sufficiently slow with respect to the spin-and-align dynamics, three-axis stabilization in the orbit frame is obtained according to Lemma 1, in the framework of singular perturbation analysis.

Remark 2 The validity of Lemma 1 stems from Theorem 11.4 in [24], which provides a local exponential stability result for the origin of a system in standard perturbation form. Nonetheless, one should note from Appendix A that the fast transient of the inner spin-and-align dynamics is almost globally stable towards the origin, whereas the nominal pitch angle control loop is linear. Hence, the nominal slow timescale dynamics is also globally stable. An extensive set of Monte Carlo simulation provides empirical evidence that, in spite of the local nature of the result used for the proof of Lemma 1, an almost global stability is achieved, with the only exception of singular configurations for the Euler angle sequence adopted in this study.

Remark 3 The system dynamics described by Eq. (22) cannot be addressed without taking into account the attitude of the spacecraft, affecting $\boldsymbol{B}$ and $\boldsymbol{D}$ through the matrix $\boldsymbol{T}_{BI}$. Nonetheless, such consideration does not hold for the proof of stability discussed in Appendix A. In fact, the presence of the attitude matrix only affects the evolution in time of the terms $\boldsymbol{B}$ and $\boldsymbol{D}$, influencing the rate of convergence toward the equilibrium, without any consequence on the asymptotic behavior of the closed-loop system.

3.3. Choice of the Control Gains

The control gains, k_ζ and k_ε, should allow for reaching the desired momentum condition in quasi-minimum time. Similarly to the cases described in [8] and [22], small values of the gains obviously result into slow convergence. On the other hand, provided the control torque is available along directions perpendicular to $\hat{\boldsymbol{b}}$ only, a high value of k_ζ and k_ϵ causes the transverse components of error signals, $\boldsymbol{Z}_\perp = (\boldsymbol{I}_3 - \hat{\boldsymbol{b}}_I \hat{\boldsymbol{b}}_I^T)\,\boldsymbol{Z}$ and $\boldsymbol{E}_\perp = (\boldsymbol{I}_3 - \hat{\boldsymbol{b}}_I \hat{\boldsymbol{b}}_I^T)\,\boldsymbol{E}$, perpendicular to the Earth magnetic field, $\hat{\boldsymbol{b}}$, to rapidly vanish. This makes the remaining components of $\boldsymbol{Z}$ and $\boldsymbol{E}$, parallel to $\hat{\boldsymbol{b}}$, converge to 0 over many revolutions. A sizing procedure is thus proposed, based on an approach similar to that presented in [8] for the detumbling maneuver, with a few relevant differences: 1) system dynamics is now represented in terms of angular momentum; 2) a non-zero value of the angular momentum, $J_2\, n$, is expected at the end of the maneuver, which in turn requires that 3) the procedure is rephrased in terms of closed loop dynamics of both $\boldsymbol{Z}_\perp$ and $\boldsymbol{E}_\perp$. The control gains are thus chosen in such a way that the variation of the transverse components of the error signals due to the control action is not faster than their variation associated to spacecraft angular rate, referred to

as rotational terms.

Let $\gamma = 0$ and assume for simplicity that $k_\zeta = k_\varepsilon = k$. The evolution of $\boldsymbol{Z}_\perp$ and $\boldsymbol{E}_\perp$, derived from Eqs. (20) and (21), is described by

$$\begin{aligned}\frac{d\boldsymbol{Z}_\perp}{dt} = (\boldsymbol{I}_3 - \hat{\boldsymbol{b}}_I\,\hat{\boldsymbol{b}}_I^T)\,\left[-k\left(\boldsymbol{I}_3 - \hat{\boldsymbol{b}}_I\,\hat{\boldsymbol{b}}_I^T\right)(\boldsymbol{Z}+\boldsymbol{E}) + \dot{\eta}\,\hat{\boldsymbol{o}}_2\right] \\ - \left[\frac{d\,\hat{\boldsymbol{b}}_I}{dt}\,\hat{\boldsymbol{b}}_I^T + \hat{\boldsymbol{b}}_I\left(\frac{d\,\hat{\boldsymbol{b}}_I}{dt}\right)^T\right]\boldsymbol{Z}\end{aligned} \tag{28}$$

$$\begin{aligned}\frac{d\boldsymbol{E}_\perp}{dt} = (\boldsymbol{I}_3 - \hat{\boldsymbol{b}}_I\,\hat{\boldsymbol{b}}_I^T)\left\{-k\left(\boldsymbol{I}_3 - \hat{\boldsymbol{b}}_I\,\hat{\boldsymbol{b}}_I^T\right)(\boldsymbol{Z}+\boldsymbol{E}) + \boldsymbol{T}_{BI}^T\,\dot{\boldsymbol{h}}_d\right. \\ \left. -\boldsymbol{T}_{BI}^T\left[\left(\boldsymbol{J}_a^{-1}\boldsymbol{T}_{BI}\boldsymbol{E}\right)\times\boldsymbol{h}_d\right]\right\} - \left[\frac{d\,\hat{\boldsymbol{b}}_I}{dt}\,\hat{\boldsymbol{b}}_I^T + \hat{\boldsymbol{b}}_I\left(\frac{d\,\hat{\boldsymbol{b}}_I}{dt}\right)^T\right]\boldsymbol{E}\end{aligned} \tag{29}$$

Remembering that the pitch angle correction task is slow with respect to the spin-and-align dynamics, one can disregard the contribution given by $\dot{\eta}$ and $\dot{\boldsymbol{h}}_d$ in Eqs. (28) and (29). Summing the two equations one has

$$\frac{d}{dt}(\boldsymbol{Z}_\perp+\boldsymbol{E}_\perp) \approx -2k\mathcal{A}\,(\boldsymbol{Z}+\boldsymbol{E}) - \boldsymbol{T}_{IO}\,\mathcal{B}\,\boldsymbol{T}_{IO}^T\,(\boldsymbol{Z}+\boldsymbol{E}) + \mathcal{C}\,(\boldsymbol{Z}+\boldsymbol{E}) + \mathcal{G}\,\boldsymbol{E} \tag{30}$$

where $\mathcal{A} = (\boldsymbol{I}_3 - \hat{\boldsymbol{b}}_I\hat{\boldsymbol{b}}_I^T)$ is the projection operator,

$$\mathcal{B} = (1/\|\boldsymbol{b}_O\|^2)\left[\dot{\boldsymbol{b}}_O\boldsymbol{b}_O^T + \boldsymbol{b}_O\dot{\boldsymbol{b}}_O^T - (2/\|\boldsymbol{b}_O\|^2)(\dot{\boldsymbol{b}}_O^T\boldsymbol{b}_O)\boldsymbol{b}_O\boldsymbol{b}_O^T\right] \tag{31}$$

and

$$\mathcal{C} = \boldsymbol{\omega}_{IO}^\times(\hat{\boldsymbol{b}}_I\hat{\boldsymbol{b}}_I^T) - (\hat{\boldsymbol{b}}_I\hat{\boldsymbol{b}}_I^T)\boldsymbol{\omega}_{IO}^\times \tag{32}$$

are related to the rotation rate of the Earth magnetic field with respect to $\mathbb{F}_I$, and $\mathcal{G} = \mathcal{A}\,\boldsymbol{T}_{BI}^T\boldsymbol{h}_d^\times\,\boldsymbol{J}_a^{-1}\boldsymbol{T}_{BI}$ is the gyroscopic term.

Following the same line of reasoning discussed in [8], it is possible to prove that, for a generic vector $\boldsymbol{v}$, it is $\|\mathcal{A}\boldsymbol{v}\| \leq \mathcal{O}(\|\boldsymbol{v}\|)$, $\|\mathcal{B}\boldsymbol{v}\| = \mathcal{O}(2n\sin\xi_m\|\boldsymbol{v}\|)$

(where the angle ξ_m represents the inclination of the spacecraft orbit relative to the geomagnetic equatorial plane [3, 30]), $\|\mathcal{C}\boldsymbol{v}\| = \mathcal{O}(n\|\boldsymbol{v}\|)$, and, finally, $\|\mathcal{G}\boldsymbol{v}\| \leq \mathcal{O}(n\|\boldsymbol{v}\|)$. All the rotational terms associated to the matrices $\mathcal{B}$, $\mathcal{C}$, and $\mathcal{G}$, are thus proportional to the orbit rate, n, whereas the control term associated to the matrix $\mathcal{A}$ is proportional to $2\,k$. Hence, neglecting the gyroscopic term $\mathcal{G}$ (for a conservative estimate in the inequality), a value of k such that

$$k < 0.5\,(1 + 2\sin\xi_m)\,n \tag{33}$$

provides a control torque which induces a variation of the transverse component of the error signals not faster than the rotational terms.

4. Numerical Validation

The control law proposed in this paper is applied to a LEO micro-satellite, equipped with a set of three mutually orthogonal MTs. The results of two simulation test cases are analyzed. The first one is related to a nominal scenario where all requirements of Lemma 1 are fulfilled, with the aim to provide a clearer insight into the timescale separation method and validate the theoretical results. In the second case the control technique is evaluated for a non-nominal spacecraft mass distribution, in the presence of external disturbances, and several control implementation issues.

4.1. Case 1: Nominal System

Table 1 shows relevant spacecraft data and orbit parameters, together with initial conditions for a sample maneuver.

A nonlinear model for spacecraft attitude dynamics is used in the simulations, where numerical propagation of Euler parameters is performed [32].

Table 1: Spacecraft and orbit data, with initial conditions for a sample maneuver.

Parameter	**Symbol**	**Value**	**Units**
Spacecraft data			
Nominal moments of inertia	$J_1^\star = J_3^\star = J_t$	1.416	kg m^2
	$J_2^\star = J_s$	2.0861	kg m^2
Maximum control dipole	$m_{\max}$	3.5	A m^2
Orbit data			
Radius (circular orbit)	r_c	7 021	km
Period	T	5710	s
Inclination	i	98	deg
Right ascension of the ascending node	$RAAN$	137	deg
Sample maneuver			
Initial Conditions	$\boldsymbol{\omega}_0$	$(0.2,\ 2,\ 0.2)^T$	deg/s
	$\psi_0,\ \phi_0,\ \theta_0$	$10, -12, -45$	deg

The initial phase during which the satellite is magnetically detumbled after injection into its orbit is not analyzed here, as it is not relevant in the framework of the present study. In all simulation test cases it is thus assumed that, after the detumbling phase [16, 23], the spacecraft angular velocity has been sufficiently reduced with respect to the initial value and the pitch axis is close to the orbit normal. Initial conditions for a sample maneuver are also reported in Table 1. The gains for the magnetic control law are selected as $k_\zeta = k_\varepsilon = \bar{k} = 0.0009$ s^{-1}, and $\lambda = \bar{\lambda} = 0.08$ rad^{-1}. The control dipole is generated as in [8], namely $\boldsymbol{m} = \boldsymbol{m}_c = \left(\hat{\boldsymbol{b}} \times \boldsymbol{M}^{(c)}\right) / \|\boldsymbol{b}\|$. It is assumed that the measurement of attitude variables is ideal and Euler angles are bounded as follows: $-\pi < \psi \leq +\pi$, $\pi < \theta \leq +\pi$ and $-\pi/2 < \phi \leq +\pi/2$.

No external disturbance is considered and a set of principal axis of inertia

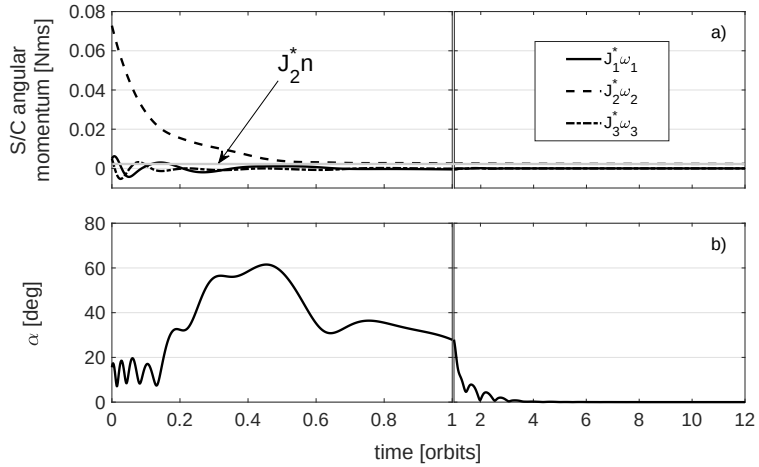

Figure 2: Pure spin acquisition and pitch axis pointing task (Case 1).

is selected as the body frame, such that $\boldsymbol{J} = \boldsymbol{J}^\star = \mathrm{diag}(J_t, J_s, J_t)$. Let $\alpha = \cos^{-1}(\hat{\boldsymbol{o}}_2 \cdot \hat{\boldsymbol{e}}_2)$ be the angular distance between the desired spin axis $\hat{\boldsymbol{e}}_2$ and the target direction, normal to the orbit plane, $\hat{\boldsymbol{o}}_2$. The time history of spacecraft angular momentum is reported in Fig. 2, where $\boldsymbol{J}\,\boldsymbol{\omega}$ rapidly converges to the desired value, $\boldsymbol{J}\,\boldsymbol{\omega}^{orb}$, while pitch-axis pointing is performed along the orbit normal, with α that approaches zero in about 4 orbits.

Time-scale separation becomes evident in Fig. 3, where Euler angles are reported. In particular, the yaw and roll angles, ψ and ϕ (that is, azimuth and elevation of the pitch axis with respect to the orbit plane, respectively) stabilize in less than 4 orbits, as it was expected from the analysis of the misalignment error α. After the initial transient, during which the excess spin rate about the pitch axis is dissipated, a slow exponential decay characterizes θ. At $t_1/T_{orb} = 4$, for example, one has $\theta(t_1) = 22.9$ deg. The number of orbits needed for the pitch angle to decrease to $\theta(t_2) = (1 - 1/e)\theta(t_1) \approx 8.4$ deg is given by $(t_2 - t_1)/T_{orb} = 1.88$, close to the nominal time constant $\tau = 1/(2\pi\lambda) = 1.99$ orbits predicted according to Eq. (42) in Appendix A.

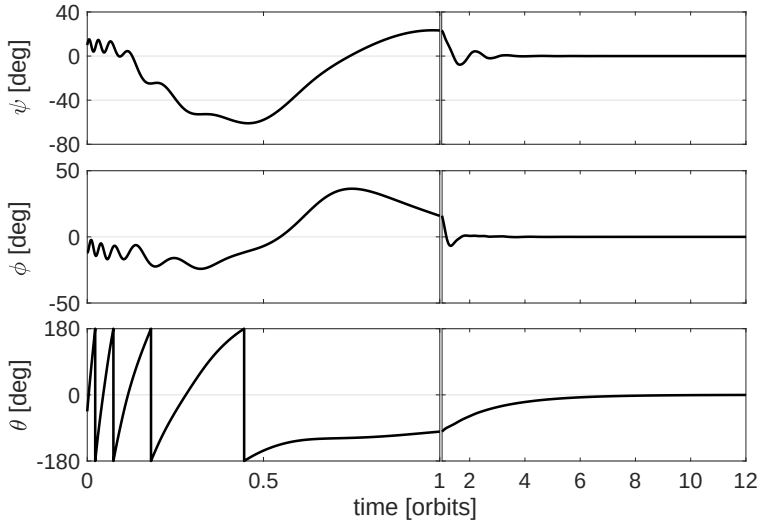

Figure 3: Spacecraft attitude error (Case 1).

A Monte Carlo approach is used as in [8] to demonstrate the validity of the control gain selection method proposed in Section 3.3 and the resulting capability of the controller to perform attitude stabilization and momentum management from arbitrary attitude conditions. Spacecraft initial attitude, angular rates, and phase along the orbit are chosen by means of a pseudo-random number generator. The same amount of angular momentum, $\|\boldsymbol{\zeta}_0\| = 0.1$ Nms, is dissipated during each Monte Carlo run. All simulations are stopped at $t = t_F$ when $\|\boldsymbol{Y}\| < (0.1 \cdot J_s\, n)$ and $|\theta| < 0.1$ deg, which represent error thresholds for fast and slow error variables, respectively.

Two sets of Monte Carlo simulations are performed. In the first set, labeled 'a', a population of 500 test cases is generated and performance in terms of convergence time t_F is reported in Fig. 4.a for different values of the gain $k_\zeta = k_\varepsilon = k$, between $\bar{k}/2$ and $2\,\bar{k}$, with $\lambda = \bar{\lambda} = 0.08$ rad^{-1}. In the same figure, the standard deviation of t_F is represented by vertical segments. Convergence time, $t_F^{(Y)}$, of the fast subsystem is reported in Fig. 4.b, repre-

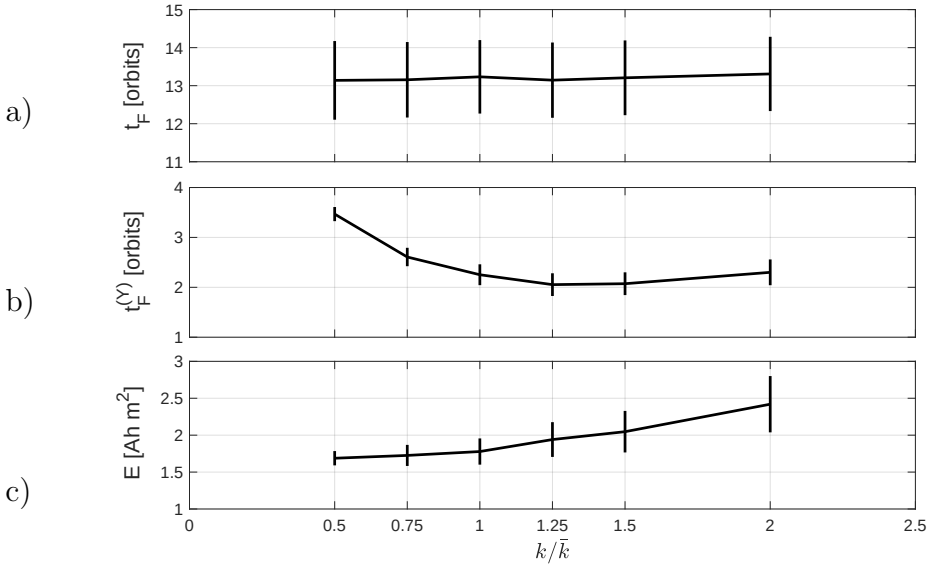

Figure 4: Performance analysis with $\lambda = 0.08$ rad^{-1}, $\bar{k} = 0.0009$ s^{-1}, and $k_\zeta = k_\varepsilon = k$ selected between $\bar{k}/2$ and $2\,\bar{k}$ (Case 1, Monte Carlo set 'a').

senting the time needed by the closed-loop system to satisfy the condition $\|\boldsymbol{Y}\| < (0.1 \cdot J_s\, n)$. For the particular selection of control gains, sufficient timescale separation is evident between the fast and the slow subsystems. In all the considered test cases, in fact, it is $t_F^{(Y)} \ll t_F$, with the convergence rate of θ depending on λ parameter only and occurring at least $5\,\tau \approx 10$ orbits after the complete stabilization of the $\boldsymbol{Y}$-error boundary-layer dynamics.

It is interesting to note that the curve representing the average value of $t_F^{(Y)}$ shows a minimum for $k = 1.25 \cdot \bar{k} = 0.0011$ s^{-1}. An increase of the gain causes a longer average convergence time, with a wider dispersion of results, whereas a sharp increase on average convergence time is evident for $k < 0.0009$ s^{-1}, following the expected behavior discussed in Section 3.3. As a last practical issue, an estimate of the maneuver cost in terms of electrical power consumption is analyzed (Fig. 4.c). Provided the magnetic dipole

moment is proportional to the current absorbed, the total electrical energy $\mathcal{E}$ necessary for completing the stabilization task is proportional to

$$\mathcal{E} \propto E = \int_0^{t_F} \left(\sum_{i=1}^{3} |m_i| \right) \mathrm{d}t \tag{34}$$

Power consumption monotonically increases with k, as expected, so that the time-optimal choice for the gain may result into a slightly heavier battery pack, with respect to a case when a smaller control gain is adopted.

In the second set of Monte Carlo simulations, labeled '*b*', performance of the closed-loop system is evaluated for different values of λ parameter, between $\bar{\lambda}/2$ and $11\,\bar{\lambda}$, with $k_\zeta = k_\varepsilon = \bar{k}$. The final convergence time, t_F, rapidly decreases with λ toward a horizontal asymptote with value approximately equal to 2.44 orbits. The latter value results to be slightly above the average convergence time, $t_F^{(Y)}$, of the fast manifold for $k_\zeta = k_\varepsilon = \bar{k}$, namely 2.25 orbits (Fig. 5.b). This means that for larger values of λ: 1) the two-timescale separation becomes less evident, with the convergence rate of $\boldsymbol{Y}$ becoming comparable to the one of θ; 2) three-axis attitude stabilization is performed in spite of the fact that timescale separation is not guaranteed; 3) dissipation of the pitch angle error still occurs after the spin-and-align maneuver task.

It is evident from the analysis of $t_F^{(Y)}$ in Fig. 5.b that convergence rate of the fast manifold depends on k only, with no significant effect induced by λ. It is interesting to note that also the total energy required is almost independent of λ (Fig. 5.c), implying that most of the energy is used to dissipate $\boldsymbol{Y}$. Only a slight increase of E is noted, provided that, for larger values of λ, the desired angular momentum $\eta(\theta) = J_s\, n\ (1 - \lambda\, \theta)$ shows major

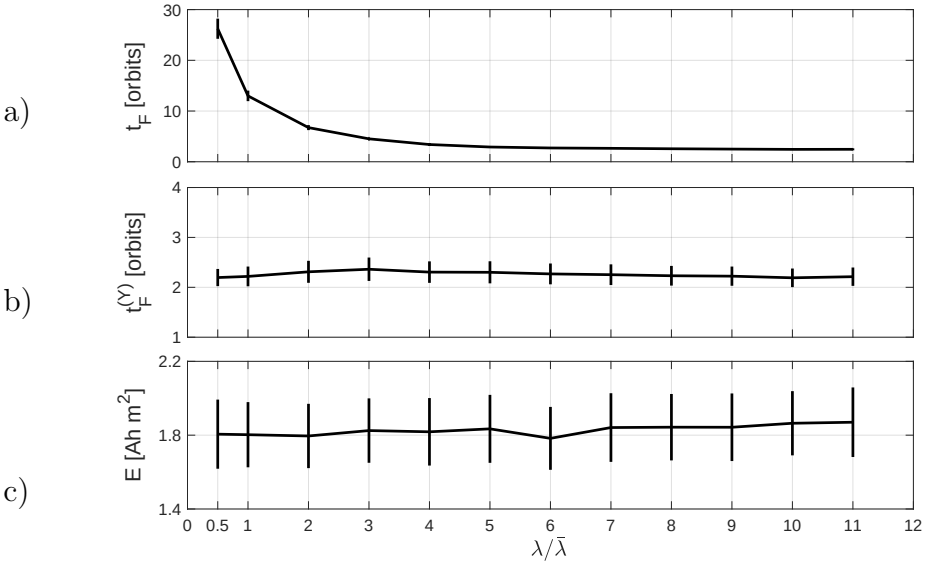

Figure 5: Performance analysis with $k_\zeta = k_\varepsilon = 0.0009$ s^{-1}, $\bar{\lambda} = 0.08$ rad^{-1}, and λ selected between $\bar{\lambda}/2$ and $11\,\bar{\lambda}$ (Case 1, Monte Carlo set '*b*').

oscillations, and more effort is required by the tracking task of the magnetic controller, with no significant reduction of final convergence time.

4.2. Case 2: Perturbed Uncertain System

Starting from the same initial conditions of Case 1, parameter uncertainties, environmental effects (gravity gradient, aerodynamic, solar radiation pressure, and residual magnetic torques) and sensor noise are included in the model for Case 2. This allows to test robustness of the closed-loop system and validate its capabilities of limiting the effects of disturbances, unmodelled dynamics, and sensor noise within acceptable pointing accuracy.

A non-nominal mass distribution, with estimated inertia matrix $\boldsymbol{J}^\star = \text{diag}(1.938, 2.086, 0.894)$ kg m^2, is adopted, which does not fulfill the requirements of Lemma 1, where axisymmetric configurations only are considered. Robustness is also demonstrated in the presence of 1) uncertainties in the

knowledge of spacecraft mass distribution and 2) off-diagonal terms in the spacecraft inertia matrix. In particular, it is assumed that the magnetic control law in Eqs. (14) and (17) is based on the knowledge of $\boldsymbol{J} = \boldsymbol{J}^{\star}$, whereas the actual spacecraft inertia matrix used in simulation is

$$\boldsymbol{J} = \begin{pmatrix} 2.0282 & 0.0127 & -0.0016 \\ 0.0127 & 2.0539 & -0.0302 \\ -0.0016 & -0.0302 & 0.8658 \end{pmatrix}$$

Aerodynamic torque is characterized by air density $\rho = 6.39 \cdot 10^{-13}$ kg/m^3 at the considered orbit altitude, with drag coefficient $C_D = 2.2$ assumed for a parallelepiped micro-satellite configuration with dimensions $L_1 = L_2 = 0.33$ m and $L_3 = 0.66$ m (respectively measured along $\hat{\boldsymbol{e}}_1$, $\hat{\boldsymbol{e}}_2$, and $\hat{\boldsymbol{e}}_3$). In this case, the face areas are given by $A_1 = A_2 = L_2\, L_3 = 0.22$ m^2 and $A_3 = L_1\, L_2 = 0.11$ m^2, while the cross-sectional area for the estimation of the drag force $\boldsymbol{F}^{(a)}$ is taken as $A = A_1$. The center of pressure, $\boldsymbol{r}_{cp} = (0.0082, 0.0030, 0.0492)^T$ m, identified for the nominal attitude [3], is assumed to be fixed in the body frame. The solar radiation pressure torque is evaluated by considering a reflectance factor $q_s = 0.8$, typical for many micro-satellite platforms, with a moment arm assumed as $\boldsymbol{r}_{srp} = \boldsymbol{r}_{cp}$. The direction of the Sun is provided in body frame components by the unit vector $\hat{\boldsymbol{s}} = \boldsymbol{T}_{BI}\,(0.578, 0.578, 0.578)^T$. The sunlit area is determined as the maximum projection area of the considered solid shape, namely $A_s = \sqrt{A_1^2 + A_2^2 + A_3^2} = 0.33$ m^2 [34], with $\hat{\boldsymbol{s}}$ normal to A_s. A residual magnetic dipole $\boldsymbol{m}_{rm} = (0.15, -0.12, -0.10)^T$ A m^2, also modeled as a constant in the body-frame, affects actuation performance.

A zero-mean Gaussian white noise is added to the nominal values of angu-

lar rate components and estimated Euler angles, with power spectral density resulting in the standard deviations 0.01 deg/s and 1.07 deg, respectively, for the sampled white noise signals. Analogous modeling is performed for magnetometer measurement noise on each axis, with standard deviation equal to 3 nT, plus the effect of a residual bias given by $(42, -12, -20)^T$ nT. The control signals are sampled at a frequency of 1 Hz, compatible with current technology of commercial MTs [36] and a first-order dynamics with a time constant $\tau_m = 20$ ms is assumed to characterize the response of each magnetic actuator. In particular, a duty-cycle of 800 ms is considered during which the MTs provide the desired control dipole. During the initial 200 ms of the sampling interval, the MTs are switched-off, allowing the onboard magnetometer sensor to perform geomagnetic field measurements, the flight management unit to compute the desired commands, and the MTs to desaturate and lessen the generated magnetic field (in this case the MTs fall time, calculated as $5\,\tau_m$, is 100 ms).

In order to improve stabilization accuracy and satisfy more stringent pointing requirements, residual dipole estimation is performed. An Extended Kalman Filter (EKF) [37] is adopted to estimate the residual dipole, $\hat{\boldsymbol{m}}_{rm}$. Recursive estimation is performed online on the basis of magnetometer readings and angular rate information, provided the latter are made available from a separate estimation task, in the framework of the main attitude and orbit determination activities. For more details about the recursive formulation of the EKF, the reader is referred to [37].

The estimator is characterized by an update time interval $\Delta t = t_k - t_{k-1} = 0.1$ s, the initial estimate is set to $\hat{\boldsymbol{x}}_0^- = \mathbf{0}_{6\times 1}$, and the predicted covariance es-

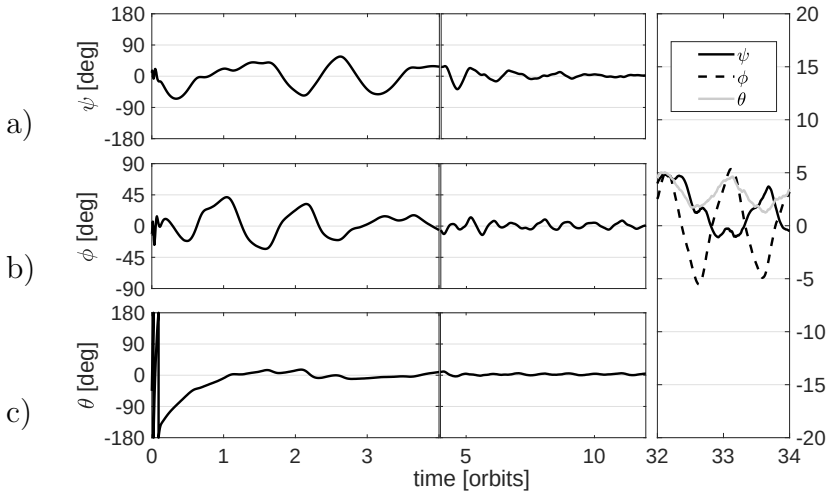

Figure 6: Spacecraft attitude error (Case 2).

timate is initialized with $\boldsymbol{P}_0^- = \text{diag}(10^{-9}, 10^{-9}, 10^{-9}, 10^{-5}, 10^{-5}, 10^{-5})$. The assigned process noise and observation noise covariance matrices are respectively given by $\boldsymbol{Q}_k = \boldsymbol{Q} = 10^{-13} \cdot \boldsymbol{I}_6$ and $\boldsymbol{R}_k = \boldsymbol{R} = 10^{-8} \cdot \boldsymbol{I}_3$ T^2. Control gains are selected in matrix form as $\boldsymbol{k}_\zeta = \boldsymbol{k}_\varepsilon = \text{diag}(0.0069, 0.0138, 0.0230)$ s^{-1} and are respectively applied to $\boldsymbol{\zeta}$ and $\boldsymbol{\varepsilon}$, while $\lambda = 0.15$ rad^{-1}. The control dipole is finally generated in order to compensate the residual dipole, provided the latter is estimated online, namely $\boldsymbol{m}_k = \boldsymbol{m}_c|_k - \hat{\boldsymbol{m}}_{rm}|_k$.

Attitude error variables, reported in Figs. 6 and 7, remain bounded in the presence of uncertainties and non-modeled disturbances. After the initial phase, during which the initial angular rates are reduced close to 0 in approximately 0.1 orbital periods, convergence towards the desired attitude is almost monotonous, achieving the desired pointing in less than 4 orbits. Such a performance compares well with other similar test cases reported in the literature, e.g. in [18], where an oscillatory behaviour of attitude variables is evident and a longer convergence time is required for achieving the

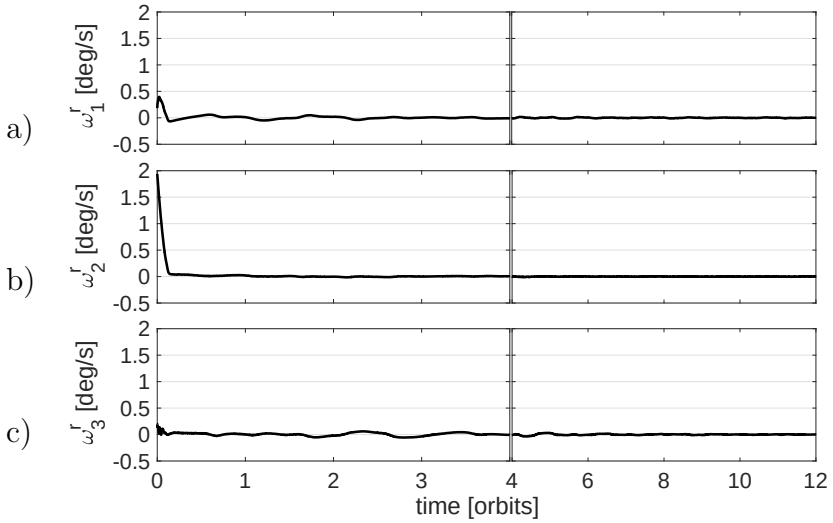

Figure 7: Spacecraft angular rates with respect to the orbit frame (Case 2).

desired pointing.

In the presence of disturbances, uncertainties and sensor noise, attitude stabilization performance in terms of yaw and roll angle errors is in the order of 2.66 and 3.13 deg 1σ, with mean values respectively given by 1.09 and 0.56 deg. A poorer but satisfactory performance is obtained for the pitch angle, characterized by only 1.42 deg 1σ error but also by a steady-state mean value of 3.21 deg (see the enlargement in Fig. 6). The residual attitude error about the pitch axis is mainly determined by the presence of the aerodynamic drag, whose lever arm is practically directed along $\hat{\boldsymbol{e}}_3$ and determines the highest torque component about $\hat{\boldsymbol{e}}_2$.

Assume that the boresight of a sensor payload or a directional antenna is directed along $-\hat{\boldsymbol{e}}_3$ and needs to be Nadir-pointed for Earth observation or communication purposes, respectively. In this scenario, $\beta = \cos^{-1}(\hat{\boldsymbol{o}}_3 \cdot \hat{\boldsymbol{e}}_3)$ is adopted to represent the Earth-pointing misalignment error, which reaches 1.58 deg 1σ error and a steady-state mean value of 4.46 deg (in the case when,

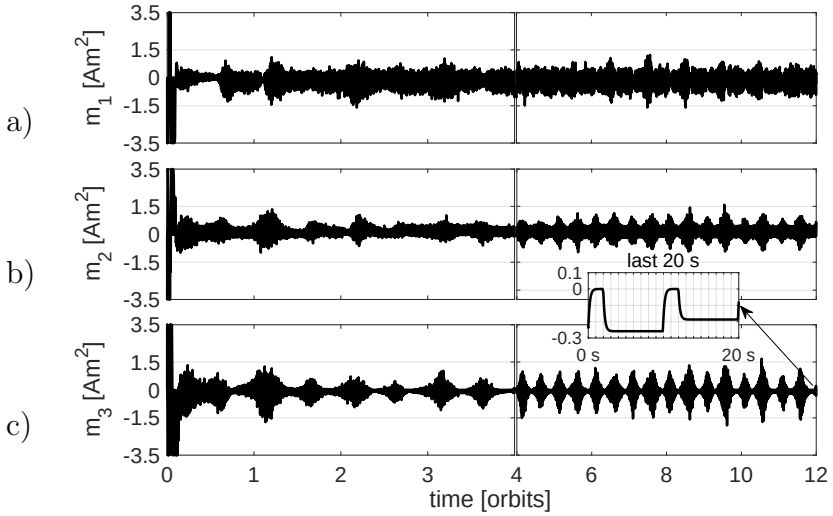

Figure 8: Dipole moment generated by the magnetorquers (Case 2).

for example, $\boldsymbol{k}_\zeta$ and $\boldsymbol{k}_\varepsilon$ are left unchanged and λ is increased from 0.15 to 0.25 rad^{-1}, note that the steady-state mean value of β reduces from 4.46 to 3.85 deg, while the error standard deviation remains practically unaltered).

Finally, spacecraft angular rates with respect to the target orbit frame oscillate with a 1σ error standard deviation of approximately 0.0036 deg/s on each axis. Statistical analysis is performed over 20 orbits in steady state conditions, demonstrating long term stability of the whole system, at the cost of keeping the MTs active with a maximum standard deviation of 0.22 A m^2, measured on m_1. The enlargement reported in the time-history of m_3 in Fig. 8 shows that, in this more realistic scenario, the MTs are activated with a frequency of 1 Hz and generate magnetic control dipoles which oscillate about the non-null values required to fully compensate the residual magnetization.

5. Conclusions

In the present work, a nonlinear control law applied to a purely magnetic-actuated Earth-pointing spacecraft is described. The stability proof is obtained under the assumption that a set of principal axes of inertia is selected as the body-fixed frame. The approach is based on a two-timescale separation of closed-loop system dynamic modes, where the acquisition of a pure spin around a prescribed principal axis of inertia, while aiming the spin axis along the orbit normal, is representative of the fast dynamics. The correction of the residual attitude error about the spin axis is performed at a slower rate for a particular choice of control parameters, thus allowing for the application of stability results from singular perturbation theory. Numerical simulations demonstrate the effectiveness of the control method for any initial attitude and validate the theoretical results. The control laws perform well in the presence of external disturbances, spacecraft inertia matrix uncertainties, and control implementation issues such as actuator saturation, control quantization, and measurement noise. The effect of magnetic residual dipoles is compensated by recursive online estimation, and satisfactory pointing accuracy is obtained for a sample small satellite mission for Earth observation.

Ackowledgments

The authors wish to express their sincerest gratitude to the anonymous reviewers, for the careful reviews received of their original manuscript, which allowed for improving the paper, making it clearer and more accurate.

Appendix A. Proof of Lemma 1

Assume that a suitable selection of control parameters λ, k_ζ, and k_ε forces the closed-loop system in Eqs. (22) and (27) to exhibit a two-timescale behavior. In particular, let the combined pure spin acquisition and spin-axis pointing tasks correspond to the fast dynamics, whose timescale is in the order of $\tau_f \propto 1/n$ (see discussion on the control gain in Section 3.3, where one requires that $k_\zeta, k_\varepsilon = \mathcal{O}(n)$). On the other hand, the correction of the residual pitch error is related to a timescale, $T_s \propto 1/(\lambda\, n)$, which can be made arbitrarily slower than τ_f, by an adequate choice of λ.

Let $x = \theta$ and $\boldsymbol{z} = \boldsymbol{Y}$ be the vectors containing the slow and the fast variables, respectively. The system in Eqs. (22) and (27) can be recast in standard form, according to the forced singular perturbation method described in [35, 38] (details are omitted for the sake of conciseness):

$$\dot{x} = f(t, x, \boldsymbol{z}, \epsilon) \tag{35}$$

$$\epsilon\, \dot{\boldsymbol{z}} = \boldsymbol{g}(t, x, \boldsymbol{z}, \epsilon) \tag{36}$$

where the perturbation parameter is a fast time constant, $\epsilon = \tau_f = 1/\min(k_\zeta, k_\varepsilon) \propto 1/n$, such that

$$f(t, x, \boldsymbol{z}, \epsilon) = \boldsymbol{Q}\ (\boldsymbol{h}_d(\theta) - \boldsymbol{T}_{BI}\, \boldsymbol{S}\, \boldsymbol{Y}) - n\, \frac{\cos\psi}{\cos\phi} \tag{37}$$

and

$$\boldsymbol{g}(t, x, \boldsymbol{z}, \epsilon) = -\epsilon\, [\boldsymbol{A}(t)\boldsymbol{K}\boldsymbol{Y} + \eta(\theta)\boldsymbol{B}\,(t, \boldsymbol{Y}) + \dot{\eta}\, \boldsymbol{D}\,(t, \boldsymbol{Y})] \tag{38}$$

Note that the spacecraft is assumed inertially axisymmetric about the pitch axis, $\hat{\boldsymbol{e}}_2$, so that for $\gamma = 0$ it is $\boldsymbol{\Delta} = \boldsymbol{0}_{3\times3}$ and, from Eq. (25), $\boldsymbol{C}\,(t, \boldsymbol{Y}) = \boldsymbol{0}_{6\times1}$. Remembering from Section 3.3 that $k_\varepsilon, k_\zeta = \mathcal{O}(n)$, the elements of the matrix

$\epsilon \boldsymbol{K}$ in Eq. (38) are $\mathcal{O}(1)$. Similarly, provided $\epsilon\,\eta(\theta) = \mathcal{O}(J_2)$, also the second term is $\mathcal{O}(1)$, given the presence of $\boldsymbol{J}_a^{-1}$ in the definition of $\boldsymbol{B}$. Conversely, the last term, $\epsilon\,\dot{\eta}\,\boldsymbol{D}\,(t, \boldsymbol{Y}) \propto \epsilon\lambda n = \mathcal{O}(\lambda)$, is vanishing, if $\lambda \ll 1$.

Given the system in Eqs. (35)-(38), the proof follows directly from the stability results for singularly perturbed systems (see Theorem 11.4 in [24]). In particular, it is $f(t, 0, \mathbf{0}_{6\times1}, \epsilon) = 0$ and $\boldsymbol{g}(t, 0, \mathbf{0}_{6\times1}, \epsilon) = \mathbf{0}_{6\times1}$. When vanishing terms are dropped, the dimension of the state space of Eqs. (35) and (36) reduces from 7 to 1, because the differential equation (36) degenerates into the algebraic equation $\mathbf{0}_{6\times1} = \boldsymbol{A}(t)\boldsymbol{K}\bar{\boldsymbol{Y}} + \eta(\theta)\boldsymbol{B}\left(t, \bar{\boldsymbol{Y}}\right)$.

The (slowly varying) desired angular momentum is assumed constant, $\bar{\eta} = \eta(\bar{\theta})$, and the latter equation is equivalent to the system

$$\dot{\bar{\boldsymbol{Z}}} = \mathbf{0}_{3\times1} = -\left[\boldsymbol{T}_{BI}^T\left(\boldsymbol{I}_3 - \hat{\boldsymbol{b}}\,\hat{\boldsymbol{b}}^T\right)\boldsymbol{T}_{BI}\right]\left(k_\zeta\,\bar{\boldsymbol{Z}} + k_\varepsilon\,\bar{\boldsymbol{E}}\right) \tag{39}$$

$$\begin{aligned}\dot{\bar{\boldsymbol{E}}} = \mathbf{0}_{3\times1} = &-\left[\boldsymbol{T}_{BI}^T\left(\boldsymbol{I}_3 - \hat{\boldsymbol{b}}\,\hat{\boldsymbol{b}}^T\right)\boldsymbol{T}_{BI}\right]\left(k_\zeta\,\bar{\boldsymbol{Z}} + k_\varepsilon\,\bar{\boldsymbol{E}}\right)\\ &-\boldsymbol{T}_{BI}^T\left[\left(\boldsymbol{J}_a^{-1}\boldsymbol{T}_{BI}\bar{\boldsymbol{E}}\right)\times(\bar{\eta}\hat{\boldsymbol{e}}_2)\right]\end{aligned} \tag{40}$$

where the degenerate angular momentum error variables $\bar{\boldsymbol{Z}}$, $\bar{\boldsymbol{E}}$ are constant vectors in $\mathbb{F}_I$, hence the error signal $\bar{\boldsymbol{e}} = k_\zeta\,\bar{\boldsymbol{Z}} + k_\varepsilon\,\bar{\boldsymbol{E}}$ is also inertially constant.

The right-hand-side of Eq. (39) is equal to the applied control torque, $\boldsymbol{M}_I = \boldsymbol{T}_{BI}^T\boldsymbol{M}$, which is zero, for any equilibrium of the degenerate system. This implies that the vector $\boldsymbol{h} = \boldsymbol{J}\boldsymbol{\omega}$ is constant in the inertial frame and only torque-free motion solutions represent admissible steady-states for the fast system. Considering the right-hand-side of Eq. (40), one has that $\dot{\bar{\boldsymbol{E}}} = \mathbf{0}_{3\times1}$ for $\boldsymbol{M}_I = \mathbf{0}_{3\times1}$ only if $\left(\boldsymbol{J}_a^{-1}\boldsymbol{T}_{BI}\bar{\boldsymbol{E}}\right)\times(\bar{\eta}\,\hat{\boldsymbol{e}}_2) = \mathbf{0}_{3\times1}$. Noting that $\boldsymbol{T}_{BI}\bar{\boldsymbol{E}} = \bar{\boldsymbol{\varepsilon}} = (-J_t\,\bar{\omega}_1, \bar{\eta} - J_s\,\bar{\omega}_2, -J_t\,\bar{\omega}_3)^T$, the cross product $\left(\boldsymbol{J}_a^{-1}\bar{\boldsymbol{\varepsilon}}\right)\times(\bar{\eta}\,\hat{\boldsymbol{e}}_2) = \mathbf{0}_{3\times1}$ if and only if $\bar{\omega}_1 = \bar{\omega}_3 = 0$, that is, a pure spin condition around $\hat{\boldsymbol{e}}_2$ is achieved.

Note that the direction of $\hat{\boldsymbol{e}}_2$ is inertially fixed, when $\boldsymbol{h} = J_s\,\bar{\omega}_2\,\hat{\boldsymbol{e}}_2$ is inertially constant, for a torque-free condition.

The angular momentum error vectors expressed in $\mathbb{F}_I$ achieve the form $\bar{\boldsymbol{E}} = (\bar{\eta} - J_s\,\bar{\omega}_2)\boldsymbol{T}_{BI}^T\hat{\boldsymbol{e}}_2$ and $\bar{\boldsymbol{Z}} = \boldsymbol{T}_{BI}^T(\bar{\eta}\,\hat{\boldsymbol{o}}_2 - J_s\,\bar{\omega}_2\,\hat{\boldsymbol{e}}_2)$. A torque-free condition can be achieved only if

1. the angular momentum error variables are such that the error signal, $\bar{\boldsymbol{e}} = k_\zeta\,\bar{\boldsymbol{Z}} + k_\varepsilon\,\bar{\boldsymbol{E}} = \boldsymbol{0}_{3\times1}$ with $\bar{\boldsymbol{Z}}, \bar{\boldsymbol{E}} \neq \boldsymbol{0}_{3\times1}$ or

2. the angular momentum error variables are such that the error signal, $\bar{\boldsymbol{e}} = k_\zeta\,\bar{\boldsymbol{Z}} + k_\varepsilon\,\bar{\boldsymbol{E}}$ remains parallel to the Earth magnetic field or

3. the equilibrium point at the origin is reached, $(\bar{\boldsymbol{Z}}^T, \bar{\boldsymbol{E}}^T)^T = \boldsymbol{0}_{6\times1}$.

Condition 1 can be achieved if and only if $k_\zeta\,\bar{\boldsymbol{Z}} = -k_\varepsilon\,\bar{\boldsymbol{E}}$, that is, $k_\zeta(\bar{\eta}\,\hat{\boldsymbol{o}}_2 - J_s\,\bar{\omega}_2\,\hat{\boldsymbol{e}}_2) = -k_\varepsilon(\bar{\eta} - J_s\,\bar{\omega}_2)\hat{\boldsymbol{e}}_2$. This, in turn, requires that $\hat{\boldsymbol{e}}_2$ and $\hat{\boldsymbol{o}}_2$ are parallel, that is $\hat{\boldsymbol{e}}_2 = \pm\hat{\boldsymbol{o}}_2$. For $\hat{\boldsymbol{e}}_2 = \hat{\boldsymbol{o}}_2$, the latter condition is satisfied if $k_\zeta(\bar{\eta} - J_s\,\bar{\omega}_2) = -k_\varepsilon(\bar{\eta} - J_s\,\bar{\omega}_2)$, which, for strictly positive gains, k_ζ and k_ε, is possible only if $\bar{\eta} - J_s\,\bar{\omega}_2 = 0$, in which case the magnitude of both error signals vanishes and Condition 3 is achieved.

The case $\hat{\boldsymbol{e}}_2 = -\hat{\boldsymbol{o}}_2$ is of little interest from both the theoretical and the practical point of view. For $\hat{\boldsymbol{e}}_2 = -\hat{\boldsymbol{o}}_2$ the spacecraft is turned upside-down with respect to the desired spin direction. Given the local nature of Theorem 11.4 in [24] such a condition represents the furthest case from the required equilibrium. At the same time this situation is unlikely to be encountered in practice, provided small values for ϕ and ψ are expected at the end of the detumbling maneuver (see Section 2.2). Hence, Condition 1

does not represent a possible equilibrium for fast states in a bounded region around the desired steady-state condition.

Condition 2 is encountered when the error signal $\bar{\boldsymbol{e}}$ becomes parallel to the direction of the local geomagnetic field vector, $\hat{\boldsymbol{b}}$, and no magnetic torque is produced. It is not possible to discard this possibility, in general, but such a condition cannot be maintained in time. For constant values of $\bar{\boldsymbol{E}}$ and $\bar{\boldsymbol{Z}}$, the direction of $\bar{\boldsymbol{e}}$ in $\mathbb{F}_I$ is constant, hence the angle between $\bar{\boldsymbol{e}}$ and the inertially–fixed direction of the normal to the orbit plane, $\hat{\boldsymbol{o}}_2$, is also constant. Conversely, even in the most elementary models of the geomagnetic field, the angle χ between $\hat{\boldsymbol{b}}$ and $\hat{\boldsymbol{o}}_2$ is time-varying. This can be easily seen for the simple dipole model, where the components of $\boldsymbol{b}$ in $\mathbb{F}_O$ are given by $\boldsymbol{b}_O = (b_1, b_2, b_3)^T = B_0\,(\cos\vartheta\,\sin i, \cos i, -2\,\sin\vartheta\,\sin i)^T$, where B_0 is magnetic field intensity, ϑ is spacecraft anomaly along the orbit, and i is orbit inclination [3]. The angle χ is given by $\chi(\vartheta) = \mathrm{atan2}(\sqrt{b_1^2 + b_3^2}, b_2)$ (where $\mathrm{atan2}(y, x)$ is the four-quadrant inverse tangent function), and the direction of $\hat{\boldsymbol{b}}$ clearly depends on ϑ, hence time t, if $i \neq 0$. In all more realistic models, such as the tilted dipole [3, 30] or the International Geomagnetic Reference Field (IGRF) [31], the direction of $\hat{\boldsymbol{b}}$ is even more erratic and does not allow for maintaining a non-trivial spin equilibrium with $\bar{\boldsymbol{e}}$ constantly parallel to $\hat{\boldsymbol{b}}$. Hence also Condition 2 is not an equilibrium for the degenerate fast system.

Excluding the case discussed for Conditions 1 and 2 (and not relevant equilibria for $\hat{\boldsymbol{e}}_2 = -\hat{\boldsymbol{o}}_2$), the degenerate solution characterizing the fast manifold is given by $\bar{\boldsymbol{z}} = \boldsymbol{h}(t, \bar{x}) = (\bar{\boldsymbol{Z}}^T, \bar{\boldsymbol{E}}^T)^T = \boldsymbol{0}_{6\times 1}$. Since $\bar{\boldsymbol{E}} = \boldsymbol{0}_{3\times 1}$, one has $\bar{\omega}_1 = \bar{\omega}_3 = 0$ (as specified above) but also $\bar{\omega}_2 = \eta(\bar{\theta})/J_2 = n\,(1 - \lambda\,\bar{\theta})$. Provided $\boldsymbol{H}_d = \eta\,\hat{\boldsymbol{\sigma}}$, where $\hat{\boldsymbol{\sigma}} = \boldsymbol{T}_{BO}\,(0, 1, 0)^T$, and taking into account the

formulation of the attitude matrix in Eq. (2), it is straightforward to prove that the solution $\bar{\boldsymbol{Z}} = \mathbf{0}_{3\times1}$ implies $\bar{\phi} = \bar{\psi} = 0$.

The functions f, $\boldsymbol{g}$, $\boldsymbol{h} = \mathbf{0}_{6\times1}$, and their partial derivatives up to second order are bounded in a neighborhood of the desired equilibrium. The degenerate solution $\bar{\boldsymbol{z}} = \boldsymbol{h}(t, \bar{x})$ is used to evaluate the unperturbed problem:

$$\dot{\bar{x}} = f(t, \bar{x}, \boldsymbol{h}(t, \bar{x}), 0) \tag{41}$$

that reduces from Eq. (27) to

$$\dot{\bar{\theta}} = -n\,\lambda\,\bar{\theta}, \tag{42}$$

the origin of which is exponentially stable. In particular, Eq. (42) appears as a first-order linear time-invariant system characterized by the time constant $\tau = 1/(n\,\lambda\,T) = 1/(2\pi\,\lambda)$, normalized by the orbit period T. Consider now the change of variable $\boldsymbol{y} = \boldsymbol{z} - \boldsymbol{h}(t, \bar{x})$ and define $\tau = t/\epsilon$. The boundary-layer system

$$\frac{d\boldsymbol{y}}{d\tau} = \boldsymbol{g}(t, \bar{x}, \boldsymbol{y} + \boldsymbol{h}(t, \bar{x}), 0) \tag{43}$$

assumes the form:

$$\frac{d\boldsymbol{y}}{d\tau} = -\boldsymbol{A}(t)\boldsymbol{K}\,\boldsymbol{y} - \boldsymbol{B}\,(t, \boldsymbol{y}) \tag{44}$$

The origin $\boldsymbol{y} = \mathbf{0}_{6\times1}$ of the system in Eq. (44) is exponentially stable, uniformly in (t, x) (the proof follows the procedure illustrated in the Appendix of [39]). Hence, according to Theorem 11.4 in [24], there exists $\epsilon^\star > 0$ such that for all $\epsilon < \epsilon^\star$, the origin of the system in Eqs. (35) and (36) is exponentially stable.

References

[1] White, J.S., Shigemoto, F.H., Bourquin, K., Satellite attitude control utilizing the Earth's magnetic field, Tech. rep. NASA-TN-D-1068, A-474 NASA Ames Research Center, Moffett Field, CA, United States (1961) 1-42.

[2] Cubas, J., de Ruiter, A.J., Magnetic control without attitude determination for spinning spacecraft, Acta Astronaut., Vol. 169, 2020, 108-123, doi: 10.1016/j.actaastro.2019.12.029

[3] Wertz, J., Spacecraft Attitude Determination and Control, Kluwer, Dordrecht, The Netherlands, 1978, Chs. 5, 17, and 19.

[4] Das, S., Sinha, M., Misra, A., Dynamic Neural Units for Adaptive Magnetic Attitude Control of Spacecraft, J. Guid. Control. Dyn., Vol. 35, No. 4, 2012, 1280-1291, doi: 10.2514/1.54408

[5] Lovera, M., Astolfi, A., Spacecraft Attitude Control Using Magnetic Actuators, Automatica, Vol. 40, No. 8, 2004, 1405-1414, doi: 10.1016/j.automatica.2004.02.022

[6] Zhou, K., Huang, H., Wang, X., Sun, L., Magnetic attitude control for Earth-pointing satellites in the presence of gravity gradient, Aerosp. Sci. Technol., Vol. 60, 2017, 115-123, doi: 10.1016/j.ast.2016.11.003

[7] Kumar, K.D., Godard, G., Abreu, N., Sinha, M., Fault-tolerant attitude control of miniature satellites using reaction wheels, Acta Astronaut., Vol. 151, 2018, 206-216, doi: 10.1016/j.actaastro.2018.05.004

[8] Avanzini, G., Giulietti, F., Magnetic Detumbling of a Rigid Spacecraft, J. Guid. Control. Dyn., Vol. 35, No. 4, 2012 1326-1334, doi: 10.2514/1.53074

[9] Mashtakov, Y., Tkachev, S., Ovchinnikov, M., Use of External Torques for Desaturation of Reaction Wheels, J. Guid. Control. Dyn., Vol. 41, No. 8, 2018 1663-1674, doi: 10.2514/1.G003328

[10] Sugita, M., Torque distribution algorithm for effective use of reaction wheel torques and angular momentums, Acta Astronaut., Vol. 139, 2017, 18-23, doi: 10.1016/j.actaastro.2017.06.014

[11] Arduini, C., Baiocco, P., Active magnetic damping attitude control for gravity gradient stabilized spacecraft, J. Guid. Control. Dyn., Vol. 20, No. 1, 1997, 117-122, doi: 10.2514/2.4003

[12] Wisniewski, R., Blanke, M., Fully magnetic attitude control for spacecraft subject to gravity gradient, Automatica, Vol. 35, No. 7, 1999, 1201-1214, doi: 10.1016/S0005-1098(99)00021-7

[13] Bushenkov, V.A., Ovchinnikov, M.Y., Smirnov, G.V., Attitude stabilization of a satellite by magnetic coils, Acta Astronaut., Vol. 50, No. 12, 2002, 721-728, doi: 10.1016/S0094-5765(02)00011-5

[14] Guelman, M., Waller, R., Shiryaev, A., Psiaki, M., Design and testing of magnetic controllers for satellite stabilization, Acta Astronaut., Vol. 56, No. 1-2, 2005, 231-239, doi: 10.1016/j.actaastro.2004.09.028

[15] Luo, W., Zhou, B., Magnetic attitude control of bias momentum spacecraft by bounded linear feedback, Aerosp. Sci. Technol., Vol. 70, 2017, 419-427, doi: 10.1016/j.ast.2017.07.047

[16] Stickler, A.C., Alfriend, K., Elementary Magnetic Attitude Control System, J. Spacecraft and Rockets, Vol. 13, No. 5, 1976, 282-287, doi: 10.2514/3.57089

[17] Cubas, J., Farrahi, A., Pindado, S., Magnetic Attitude Control for Satellites in Polar or Sun-Synchronous Orbits, J. Guid. Control. Dyn., Vol. 38, No. 10, 2015, 1-12, doi: 10.2514/1.G000751

[18] Psiaki, M.L., Magnetic torquer attitude control via asymptotic periodic linear quadratic regulation, J. Guid. Control. Dyn., Vol. 24, No. 2, 2001, 386-394, doi: 10.2514/2.4723

[19] Lovera, M., Marchi, E.D., Bittanti, S., Periodic attitude control techniques for small satellites with magnetic actuators, IEEE Trans. Control Syst. Technol., Vol. 10, No. 1, 2002, 90-95, doi: 10.1109/87.974341

[20] Steyn, W.H., Comparison of low-earth-orbit satellite attitude controllers submitted to controllability constraints, J. Guid. Control. Dyn., Vol. 17, No. 4, 1994, 795-804, doi: 10.2514/3.21269

[21] Lovera, M., Astolfi, A., Global magnetic attitude control of inertially pointing spacecraft, J. Guid. Control. Dyn., Vol. 28, No. 5, 2005, 1065-1072, doi: 10.2514/1.11844

[22] Avanzini, G., de Angelis, E.L., Giulietti, F., Acquisition of a Desired Pure Spin Condition for a Magnetically Actuated Spacecraft, J. Guid. Control. Dyn., Vol. 36, No. 6, 2013, 1816-1821, doi: 10.2514/1.59364

[23] Avanzini, G., de Angelis, E.L., Giulietti, F., Spin-axis pointing of a

magnetically actuated spacecraft, Acta Astronaut., Vol. 94, No. 1, 2014, 493-501, doi: 10.1016/j.actaastro.2012.10.035

[24] Khalil, H.K., Nonlinear Systems, Third Edition, Prentice Hall, Upper Saddle River, NJ, 2002, Ch. 11.

[25] Adams, J.J., Bergeron, H.P., and Howell, W.E., Simulator study of a satellite attitude control system using inertia wheels and a magnet, NASA Technical Note NASA-TN-D-1969, 1963, 1-16.

[26] Bayat, F., Conceptual design of a low-cost real-time hardware-in-the-loop simulator for satellite attitude control system, Turk. J. Elec. Eng. & Comp. Sci., Vol. 23, 2015, 789-803, doi: 10.3906/elk-1212-20

[27] Celani, F., Spacecraft Attitude Stabilization with Piecewise-Constant Magnetic Dipole Moment, J. Guid. Control. Dyn., Vol. 39, No. 5, 2016, 1137-1142, doi: 10.2514/1.G001388

[28] Bayat, F., Model Predictive Sliding Control for Finite-Time Three-axis Spacecraft Attitude Tracking, IEEE Transactions on Industrial Electronics, Vol. 66, No. 10, 2019, 7986-7996, doi: 10.1109/TIE.2018.2881936

[29] Xu, S., Wen, H., Huang, Z., Robust fuzzy sampled-data attitude control of spacecraft with actuator saturation and persistent disturbance, Aerosp. Sci. Technol., Vol. 101, 2020, 105850, doi: 10.1016/j.ast.2020.105850

[30] Hablani, H., Comparative Stability Analysis and Performance of Magnetic Controllers for Bias Momentum Satellites, J. Guid. Control. Dyn., Vol. 18, No. 6, 1995, 1313-1320, doi: 10.2514/3.21547

[31] International Geomagnetic Reference Field, http://www.ngdc. noaa. gov/IAGA/vmod/igrf.html [retrieved on August 1st, 2014].

[32] Wie, B., Space Vehicle Dynamics and Control, 2nd Edition, American Institute of Aeronautics and Astronautics, Inc., Reston, VA, 2008, Ch. 5.

[33] Starin, S.R., Eterno, J., Attitude Determination and Control Systems, NASA Technical Report Nr. 20110007876, 2011, Ch. 19.1.

[34] Saucier, R., Resolving the Orientation of Cylinders and Cuboids from Projected Area Measurements, US Army Research Laboratory Report Nr. ARL-TN-0759, 2016, 1-34.

[35] Naidu, D.S., Calise, A.J., Singular Perturbations and Time Scales in Guidance and Control of Aerospace Systems: A Survey, J. Guid. Control. Dyn., Vol. 24, No. 6, 2001, 1057-1078, doi: 10.2514/2.4830

[36] Nakajima, Y., Murakami, N., Ohtani, T., Nakamura, Y., Hirako, K., Inoue, K., SDS-4 Attitude Control System: In-Flight Results of Three Axis Attitude Control for Small Satellites, IFAC Proceedings Volumes, Vol. 46, No. 19, 2013, 283-288, doi: 10.3182/20130902-5-DE-2040.00077

[37] Inamori, T., Sako, N., Nakasuka, S., Magnetic dipole moment estimation and compensation for an accurate attitude control in nano-satellite missions, Acta Astronaut., Vol. 68, 2011, 2038-2046, doi: 10. 1016/j.actaastro.2010.10.022

[38] Narang-Siddarth, A., Valasek, J., Nonlinear Time Scale Systems in Standard and Nonstandard Forms: Analysis and Control, Society for Industrial and Applied Mathematics, Philadelphia, PA, 2014, Ch. 1.

[39] de Angelis, E.L., Giulietti, F., de Ruiter, A.H.J., Avanzini, G., Spacecraft Attitude Control Using Magnetic and Mechanical Actuation, J. Guid. Control. Dyn., Vol. 39, No. 3, 2016, 564-573, doi: 10.2514/1.G000957